View metadata, citation and similar papers at core.ac.uk

brought to you by CORE

provided by NASA Technical Reports Server

DYNAMIC ANALYSIS OF MULTI-DEGREE-OF-FREEDOM SYSTEMS USING PHASING MATRICES

Richard L. Bielawa*
United Aircraft Research Laboratories
East Hartford, Connecticut

Abstract

A mathematical technique is presented for improved analysis of a wide class of dynamic and aeroelastic systems characterized by several degrees-of-freedom. The technique enables greater utilization of the usual eigensolution obtained from the system dynamic equations by systematizing the identification of destabilizing and/or stiffening forces. Included, as illustrative examples of the use of the technique, are analyses of a helicopter rotor blade for bending-torsion divergence and flutter and for pitch-lag/flap instability.

Notation

$[A]$, $[B]$, $[C]$	Inertia, damping and stiffness matrices, respectively, Eq. (1)
A_{v_k}	Pitch-lag coupling for k'th edgewise mode $(=\Delta\theta/\Delta q_{v_k})$
A_{w_m}	Pitch-flap coupling for m'th flatwise mode $(=\Delta\theta/\Delta q_{w_m})$
a	Section lift curve slope, /rad
a_{ij}, b_{ij}, c_{ij}	Elements of the [A], [B] and [C] matrices
C_{e_k}	Viscous equivalent structural damping of k'th edgewise mode
c	Blade chord, in.
EI_y, EI_z	Flatwise and edgewise bending stiffness, respectively, lb-in.^{2}
$\{F(t)\}$	Dynamic excitation force vector, Eq. (1)
f_n	Resultant driving force for n'th degree of freedom, Eq. (5)
$[G(\lambda_i)]$	Dynamic matrix for i'th eigenvalue, Eq. (3)
GJ	Torsional stiffness, lb-in.^{2}
K_c	Root feathering spring, in.-lb/rad
k_A	Polar radius of gyration of spar about its center, in.
$k_{y_{lo}}$, $k_{z_{lo}}$	Section thickness-wise and chordwise mass radii of gyration, respectively, about spar center, in.
m	Section mass distribution, lb-sec^2/in.^{2}
m_o	Reference mass distribution, (= 0.000776 lb-sec^2/in.^{2})
$[P_{A_i}]$, $[P_{B_i}]$, $[P_{C_i}]$	"Stability" Force Phasing Matrices for i'th eigenvalue, Eqs. (6) through (8)
$[\hat{P}_{A_i}]$, $[\hat{P}_{B_i}]$, $[\hat{P}_{C_i}]$	"Stiffness" Force Phasing Matrices for i'th eigenvalue, Eqs. (10) through (13)
q_{v_k}	k'th edgewise modal response variable
q_{w_i}	i'th flatwise modal response variable
q_{θ_j}	j'th torsional modal response variable, (j = 1, for rigid feathering)
R	Rotor radius, in.
r	Blade spanwise location, in.
T	Tension at r, lb
t	Time, sec
$\{x\}$	Vector of degrees of freedom
$y_{lo_{cg}}$, $y_{lo_{c/4}}$, $y_{lo_{3c/4}}$	Chordwise positions forward of spar center of mass center, quarter chord, and three-quarter chord, in.
α_o	Spanwise variable section angle of attack about which perturbations occur, rad
β	Blade pre-coning angle, rad
γ_i	Angle defined in Fig. 1 (= arg λ_i)
γ_{v_k}	k'th assumed edgewise mode shape
γ_{w_i}	i'th assumed flatwise mode shape
γ_{θ_j}	j'th assumed torsion mode shape
δ_o, δ_4	Coefficients describing quartic variation of profile drag coefficient with angle of attack
δ_{ij}	Kronecker delta
η	Number defined in Eq. (9)
θ	Geometric (collective) pitch angle at r, rad
θ_e	Elastic torsion deflection at r, rad
λ	(Uniform) rotor inflow
λ_i	i'th eigenvalue, /sec
ρ	Air density, lb-sec^2/in.^{4}
σ	Blade solidity
σ_i	Real part of i'th eigenvalue, /sec
$\{\phi^{(i)}\}$	i'th eigenvector of dynamic matrix equation
Ω	Rotor rotational speed, rad/sec
ω_i	Imaginary part of i'th eigenvalue, /sec

*Senior Research Engineer, Rotary Wing Technology Group.

$(^*)$	Differentiation with respect to (Ωt)
$(\ )'$	Differentiation with respect to r
$(\bar{\ })$	Indicates quantity is nondimensionalized using combinations of R, m_o and Ω, as appropriate
$[\ ]$	Diagonal matrix

I. Introduction

Dynamic and aeroelastic analyses of aerospace structures typically involve deriving and solving sets of linear differential equations of motion generally written in matrix form:

$$[A]\{\ddot{x}\} + [B]\{\dot{x}\} + [C]\{x\} = \{F(t)\} \qquad (1)$$

In general, the A, B and C matrices are square and real-valued. A recognized hallmark of rotary wing and turbomachinery dynamics is an abundance of nonconservative forces (usually involving rotor rotation speed). Consequently, the resulting analyses produce matrix equations of motion of the above type which are highly nonsymmetrical, and often of large orders.

Although a large part of the dynamic analyst's job involves the calculation of dynamic loads and stresses due to explicit excitations, the scope of this paper will be limited to the equally important eigenproblem (F(t) = 0):

$$\{x\} = \sum_i \{\varphi^{(i)}\} e^{\lambda_i t} \qquad (2)$$

$$\left[[A]\lambda_i^2 + [B]\lambda_i + [C]\right]\{\varphi^{(i)}\} = [G(\lambda_i)]\{\varphi^{(i)}\} = \{0\} \qquad (3)$$

The eigenvalues λ $(= \sigma \pm i\omega)$, which give stability and natural frequency information are obtained from the familiar characteristic determinant:

$$|[A]\lambda^2 + [B]\lambda + [C]| = 0 \qquad (4)$$

by any of various well-established methods [1], [2], [3]. The "flutter" mode shapes, $\phi^{(i)}$, are obtained from Eq. (3) once the eigenvalues are known.

This paper presents an easily implemented technique for the improved analysis of dynamic systems of the type described above. The technique requires a reliable eigensolution and involves manipulations of the given dynamic equations, their eigenvalues and eigenvectors. Specifically, the technique systematizes the identification of destabilizing and/or stiffening forces by the calculation of "force phasing matrices". Applications of the technique to analyses of bending-torsion divergence and flutter and of pitch-lag/flap instability of a helicopter rotor blade are presented. Furthermore, this paper essentially represents an expansion of a portion of an earlier paper [4].

II. Mathematical Development

The principal function of the force-phasing matrix technique is to identify those force terms in the equations of motion which, for an unstable mode, are so phased by the mode shape as to be drivers of the motion. The technique is perhaps nothing more than a formalization of the intuitive use an experienced dynamicist would make of the eigenvector information. The basis of the technique can be seen by writing any single equation of the set represented by Eq. (3) as the sum of the mass, damper and spring forces of the diagonal degree-of-freedom and the remaining forces acting as a combined exciting force.

$$a_{nn}\lambda_i^2\varphi_n^{(i)} + b_{nn}\lambda_i\varphi_n^{(i)} + c_{nn}\varphi_n^{(i)} + \underbrace{\sum_{j\neq n}(a_{nj}\lambda_i^2 + b_{nj}\lambda_i + c_{nj})\varphi_j^{(i)}}_{f_n} = 0 \qquad (5)$$

For the usual case a_{nn}, b_{nn} and c_{nn} are all positive numbers; that is, each mass when uncoupled from the others is a stable spring-mass-damper system. Since the root, λ_i, is generally complex, Eq. (5) can then be interpretted as the sum of four complex quantities or vectors in the complex plane which must, furthermore, be in equilibrium. Assuming that the root with positive imaginary part is used throughout, the argument of the root, γ_i, is the angle by which the inertia force vector is rotated relative to the damper force vector and the damper force vector is rotated relative to the spring force vector. For an unstable root this angle will be less than 90 degrees. If a purely imaginary value is assigned to the spring force vector, unstable motion is assumed and it is recalled that the four vectors are in equilibrium, then

the real parts of the damper and inertia force vectors will be negative and the driving force must always have a positive real part. Figure 1, which demonstrates this argument, shows the four force vectors in the complex plane for an unstable oscillatory mode ($Re(\lambda_i) = \sigma_i > 0$) and for unit imaginary displacement:

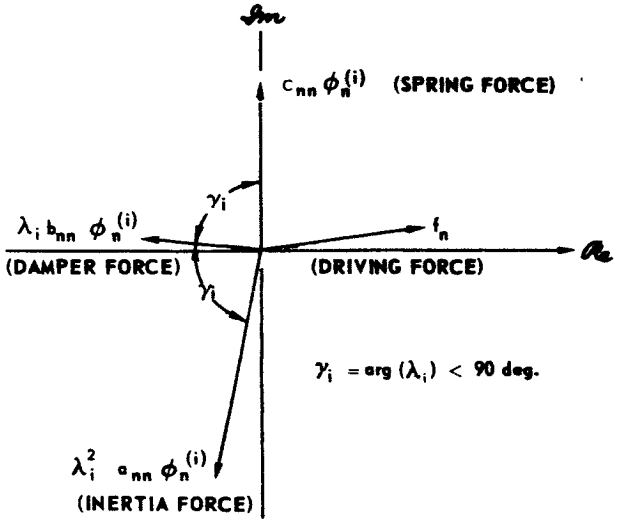

Figure 1. Force-Vector Diagram for n'th Degree-Of-Freedom, i'th Mode (Oscillatory Instability)

A secondary function of the technique is to identify those terms in the equations which, for any coupled mode, act as stiffness so as to increase the coupled frequency of the mode. Reference to Figure 1 shows that driving forces with positive imaginary parts will tend to reinforce the diagonal spring term and, hence, raise the frequency of the coupled mode. An interesting observation that can be made from Figure 1 is that, for unstable motion, the diagonal damper force also has a positive imaginary part. Hence, it tends to stiffen the (unstable) coupled mode in contrast to the frequency lowering effect of damping for stable motion.

Figure 2 shows the same forces as vectors for an unstable aperiodic mode (divergence) for negative unit real displacement:

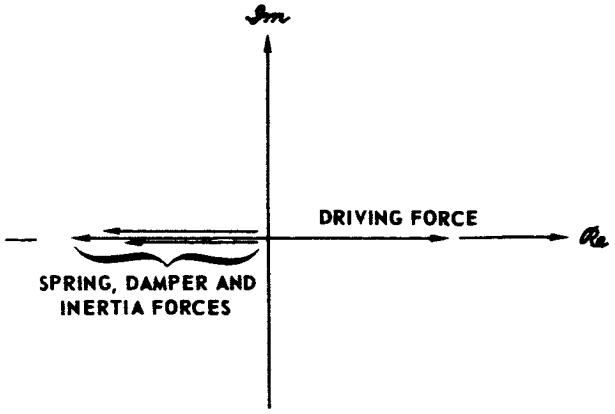

Figure 2. Force-Vector Diagram for n'th Degree-of-Freedom, Divergence Instability.

Again, the driving force is always a positive real number. Furthermore, for divergences, stiffening forces are by definition stabilizing; hence, those components of the driving force which are negative are also those that stiffen the coupled mode.

These interpretations of unstable motion can be quantitatively implemented first, by multiplying each of the dynamic equations (i.e., each row of the equation (1)) by a quantity which makes the diagonal stiffness force (stiffness matrix element x displacement) become pure imaginary and second, by representing the modal vector as a diagonal (square) matrix. This latter operation has the effect of evaluating the magnitudes of the component dynamic equation forces without numerically adding them together. The resulting "stability" force phasing matrices are then readily written as:

$$[P_{A_i}] = Re[\eta/\varphi^{(i)}]\lambda_i^2[A][\varphi^{(i)}] \quad (6)$$

$$[P_{B_i}] = Re[\eta/\varphi^{(i)}]\lambda_i[B][\varphi^{(i)}] \quad (7)$$

$$[P_{C_i}] = Re[\eta/\varphi^{(i)}][C][\varphi^{(i)}] \quad (8)$$

where

$$\eta = \begin{cases} 1 & \text{, for oscillatory instabilities} \\ -1. & \text{, for divergences} \end{cases} \quad (9)$$

and where the eigenvalue in the upper half plane is used.

In all cases, the real parts of the above indicated matrix expressions give instability driving force information. Forces defined by elements of the A, B and C dynamic equation matrices which are phased by the mode shape so as to be drivers of the motion then cause the corresponding elements of the P_{Ai}, P_{Bi} and P_{Ci} "stability" force phasing matrices, respectively, to be positive and proportional to their strength as drivers.

Stiffening driving force information is obtained differently for oscillatory motion and for aperiodic motion. Those elements of the dynamic equation matrices which are phased so as to be stiffeners of the coupled mode will cause the corresponding elements of the matrix expressions to be either positive imaginary for oscillatory motion, or negative real for aperiodic motion. The resulting "stiffness" force phasing matrices are then expressed as:

$$[\hat{P}_{A_i}] = \mathrm{Im}[\eta/\varphi^{(i)}]\lambda_i^2[A][\varphi^{(i)}] \qquad (10)$$

$$[\hat{P}_{B_i}] = \mathrm{Im}[\eta/\varphi^{(i)}]\lambda_i[B][\varphi^{(i)}] \qquad (11)$$

$$[\hat{P}_{C_i}] = \mathrm{Im}[\eta/\varphi^{(i)}][C][\varphi^{(i)}] \qquad (12)$$

for oscillatory motion, and:

$$[\hat{P}_{(\ )_i}] = [P_{(\ )_i}] \qquad (13)$$

for aperiodic motion.

It should be stressed that these force phasing matrices are no more than a more systematic and efficient interpretation of the all too often voluminous eigensolution information. The following sections illustrate the usage of the force phasing matrix technique in substantiating what is generally known of some rather fundamental, classical helicopter rotor blade instabilities.

III. Description of Illustrative Rotor Blade Example

For illustrative purposes, relatively simple linear equations of motion were formulated for a generalized untwisted helicopter rotor blade and then applied to a realistic nonarticulated rotor configuration. The blade is assumed to be operating in an unstalled hover condition at some collective angle and with a built-in coning angle. Perturbative elastic flatwise, edgewise and torsion motions are assumed to occur about the preconed position. The resulting linear aeroelastic equations are fairly standard [5], [6]; quasi-static aerodynamics (uniform inflow) is assumed and a normal mode description of the blade elasticity is employed. Thus, for the chosen configuration, two flatwise bending modes, one edgewise bending mode, and the rigid feathering degree-of-freedom are assumed. The resulting response vector, $\{x\}$, consists of the quantities q_{w1}, q_{w2}, q_{v1}, and $q_{\theta 1}$ whose detailed dynamic equations are given in the Appendix. The dynamic equations then comprise a set of four differential equations written as a 4 x 4 matrix equation of the Eq. (1) type. The aeroelastic degrees-of-freedom together with the general parameters are shown in Figure 4:

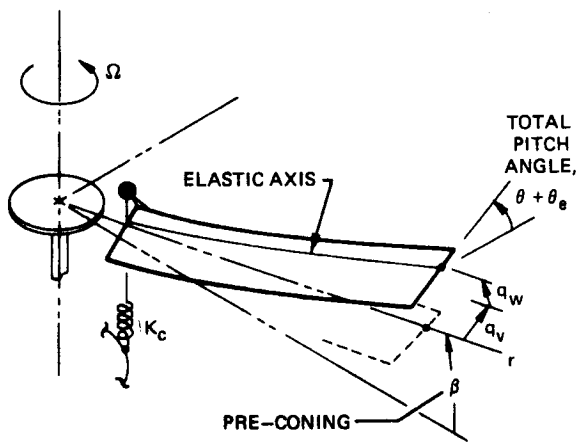

Figure 4. Schematic of Nonarticulated Rotor Configuration and Aeroelastic Degrees-of-Freedom.

The basic configuration incorporates a counterweight over the outer 70 percent of the blade, pitch-flap coupling (determined from the geometry of the pushrod attachment and flatwise modal deflection) and pitch-lag coupling of arbitrary magnitude. The chordwise position of the counterweight and the magnitude of pitch-lag coupling are purposely varied in the following analysis to establish known blade instabilities in order to illustrate the phasing matrix analysis technique. Table I below summarizes the pertinent geometric and aeroelastic data for the rotor blade configuration:

TABLE I - BLADE CHARACTERISTICS

Radius	210 in.
Chord (0.1R to tip)	13.5 in.
Tip Speed	650 fps
Pitch-Flap coupling, A_{w_m} $\begin{cases} m = 1 \\ m = 2 \end{cases}$	$\begin{matrix} 0. \\ 0.188 \end{matrix}$
Roof feathering spring rate	3.55×10^6 in.-lb/rad
Blade coning	2 deg.
Airfoil: (NACA 0012; Mach No. = 0):	
a	6.0/rad
δ_0	0.01
δ_4	3.30/rad^4
(Uniform) mass distribution	0.000776 lb-sec^2/in.^{2}
(Uncoupled) blade natural frequencies:	
first flatwise mode	1.092/rev
second flatwise mode	2.681/rev
first edgewise mode	1.390/rev
rigid feathering	3.820/rev
$\frac{\text{(edgewise mode structural damping)}}{\text{(critical damping)}}$	0.01
Flight condition (hovering)	sea level, standard
collective angle, θ	10 deg.
inflow ratio, λ	-.0601

The normal flatwise and edgewise mode shapes used are shown in Figure 5.

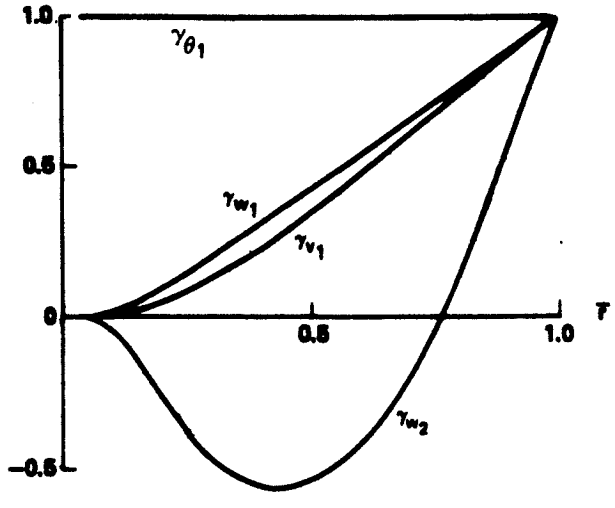

Figure 5. Spanwise Variation of Normal Mode Shapes.

IV. Application of Analysis to Illustrative Example

Basic Configuration

For purposes of comparison, the data in Table I was used together with a collective angle of 10 deg, inflow ratio of -0.0601, and with zero counterweight chordwise offset (from the quarter chord), and zero pitch-lag coupling. This basic case is stable in all modes as is shown by the following list of resulting eigenvalues:

$$\lambda_{1,2} = -0.504 \pm i0.960$$
$$\lambda_{3,4} = -0.411 \pm i2.610$$
$$\lambda_{5,6} = -0.027 \pm i1.398$$
$$\lambda_{7,8} = -1.472 \pm i3.506$$

While all the aeroelastic modes represented by the various eigenvalues comprise responses in all the four degrees of freedom, they could be characterized as follows: mode 1 ($\lambda_{1,2}$) is first flatwise bending, mode 2 ($\lambda_{3,4}$) is second flatwise bending, mode 3 ($\lambda_{5,6}$) is first edgewise bending, and mode 4 ($\lambda_{7,8}$) is rigid feathering.

Configuration With Rearward Chordwise Counterweight

If the 70 percent outer span counterweight is artificially shifted aft so as to place the chordwise section mass center at the 32 percent chord point, reference to the dynamic equations (A-1, A-2 and A-3) then yields the following A, B and C matrices (given in E format):

A (Inertia) Matrix:

.2909-00	-.0000	-.0000	-.1884-02
-.0000	.2006-00	-.0000	.3482-03
-.0000	-.0000	.2542-00	-.0000
-.1884-02	.3482-03	-.0000	.1133-03

B (Damping) Matrix:

.2887-00	.7757-01	-.4500-02	-.1256-01
.7992-01	.1665-00	-.8166-02	-.3309-03
.3099-01	.1943-01	.7901-02	-.2020-02
.1536-07	.6326-04	-.1058-03	.3370-03

C (Stiffness) Matrix:

.3382-00	-.5763-01	.4633-01	-.3067-00
-.8232-03	.1422+01	.7484-02	-.7080-01
.4633-01	-.2974-02	.4988-00	-.4396-01
-.2300-02	-.5423-02	-.2919-03	.1646-02

The first two rows of the matrix equation are the equations for the first and second flatwise bending modes, respectively. The third

row is the equation for the first edgewise mode, while the fourth is for rigid feathering. Correspondingly, elements in the first two columns of the matrices are terms multiplying the flatwise bending responses and their derivatives. Similarly, third and fourth column elements are terms multiplying edgewise bending and rigid feathering, respectively, and their derivatives.

The eigensolution for these matrices (see Eq. (4)) reveals the configuration to be unstable in both divergence and flutter:

$$\lambda_{1,2} = 0.408, \quad -4.466$$
$$\lambda_{3,4} = 0.300 \pm i1.789$$
$$\lambda_{5,6} = -0.0088 \pm i1.402$$
$$\lambda_{7,8} = -0.578 \pm i3.099$$

Since the equations are in nondimensional form, the units of these eigenvalues are per rotor revolution frequency or "p". Using Eqs. (6) through (9) the following "stability" force phasing matrices are written for the unstable divergence mode:

A Phasing Matrix, P_{A_1}

-.4840-01	-.0000	-.0000	.5061-03
-.0000	-.3338-01	-.0000	-.1726-02
-.0000	-.0000	-.4229-01	-.0000
.1941-03	-.1944-05	-.0000	-.1885-04

B Phasing Matrix, P_{B_1}

-.1178+00	-.1715-02	.4408-04	.9272-02
-.6016-00	-.6791-01	.1476-02	.4022-02
-.5265-00	-.1789-01	-.3223-02	.5540-01
-.3881-08	-.8660-06	.6418-06	-.1375-03

C Phasing Matrix, P_{C_1}

-.3382-00	.3123-02	-.1113-02	.4953-00
.1519-01	-.1422+01	-.3316-02	.2110+01
-.1929+01	.6710-02	-.4988-00	.2956+01
.1424-02	.1820-03	.4341-05	-.1646-02

The larger of the destabilizing driving forces, which show up as positive terms, have been underlined for clarity. A reasonable yard-stick for measuring the size of the destabilizing forces is to compare them to the size of the stabilizing element in each matrix equation row. For oscillatory instabilities that element would be the diagonal damping force; for divergences, it would be the diagonal stiffness force. As would be expected of a divergence instability, the major destabilizing forces are displacement dependent (i.e., appear in the C matrix). By making additional reference to Eqs. (A-1) and (A-2), and (A-3) and to their evaluation given above, the following interpretation can be drawn from these results:

1. The unstable mechanism involves a coupling mainly between first flatwise bending and rigid feathering. The mode shape, $\phi^{(1)}$ = (0.619, 0.0336, 0.0149, and 1.0), confirms this result.

2. The position of the chordwise mass center behind the elastic axis, as indicated by negative dynamic equation elements $a_{1,4}$ and $c_{4,1}$ and reference to the explicit statements of the equations in the Appendix, is a major link in the unstable coupling chain of events. This result confirms well-known results concerning the divergence of rotor blades [5]; specifically, that the torsion modes drive the flatwise modes aerodynamically (elements $c_{1,4}$ and $c_{2,4}$) while the flatwise modes drive the torsion modes with centrifugal inertial forces through the rearward mass center position (elements $c_{4,1}$ and $c_{4,2}$).

3. The first edgewise bending mode is being driven by the rigid feathering through aerodynamic and inertia terms (element $b_{3,4}$) but is not actively participating in the unstable mechanism.

In a similar manner the following force phasing matrices are written for the unstable oscillatory (flutter) mode, λ_3:

A Phasing Matrix, P_{A_3}

-.3125-00	-.0000	-.0000	-.1904-01
-.0000	-.2155-00	-.0000	-.1101-01
-.0000	-.0000	-.2731-00	-.0000
.1421-02	-.1114-04	-.0000	-.1217-03

B Phasing Matrix, P_{B_3}

-.5163-00	.7587-02	.2749-02	-.1968-01
.6947-00	-.2978-00	-.1561-01	.1282-01
-.1493-00	.1659-02	-.1413-01	-.4186-05
.5201-08	-.5155-05	-.6870-05	-.6027-03

C Phasing Matrix, P_{C_3}

-.1260-08	.6779-02	-.4386-02	.8548-00
-.4997-02	-.1325-08	.1751-01	-.1802-00
.3814-01	.1173-02	-.0000	.3956-00
-.6696-03	.2794-04	-.3155-04	-.0000

Again the major destabilizing terms have been underlined for clarity. With few exceptions the same interpretations can be made of the flutter force phasing matrices as were made for the divergence ones. While the feathering

degree-of-freedom again drives the first flatwise mode aerodynamically (element $c_{1,4}$), the flatwise mode now drives the feathering degree-of-freedom with vibratory inertia forces (element $a_{4,1}$). Again these results confirm well-known findings.

Configuration With Pitch-Lag Coupling

Using the reconfirmed knowledge that an aft chordwise center of mass is destabilizing, the configuration is altered back to the original quarter chord balanced configuration. In addition, unit pitch-lag coupling ($A_{v_1} = 1.$) is introduced into the configuration. The resulting dynamic equations are as follows:

A (Inertia) Matrix

.2909-00	-.0000	-.0000	-.0000
-.0000	.2006-00	-.0000	-.0000
-.0000	-.0000	.2542-00	-.0000
-.0000	-.0000	-.0000	.1133-03

B (Damping) Matrix

.2887-00	.7757-01	-.1622-01	-.1256-01
.7992-01	.1665-00	-.8596-02	-.3309-03
.3015-01	.1953-01	.1003-01	-.2169-02
.1536-07	.6326-04	.3801-03	.3370-03

C (Stiffness) Matrix

.3382-00	-.5763-01	-.2563-00	-.3049-00
-.8232-03	.1422+01	-.5358-01	-.7113-01
.4633-01	-.2974-02	.4431-00	-.4337-01
-.0000	-.0000	-.0000	.1646-02

The eigenvalues for this configuration reveal the configuration to be unstable in the edgewise bending mode:

$\lambda_{1,2} = -0.573 \pm i0.977$
$\lambda_{3,4} = -0.408 \pm i2.609$
$\lambda_{5,6} = 0.0119 \pm i1.324$
$\lambda_{7,8} = -1.449 \pm i3.505$

Again, the stability force-phasing matrices are formed for the unstable mode (λ_5) and the larger positive terms are underlined:

A Phasing Matrix, P_{A_5}

-.9137-02	-.0000	-.0000	-.0000
-.0000	-.6302-02	-.0000	-.0000
-.0000	-.0000	-.7985-02	-.0000
-.0000	-.0000	-.0000	-.3558-05

B Phasing Matrix, P_{B_5}

-.3822-00	.5003-02	-.2424-01	.8736-02
.2114+01	-.2204-00	.2079-00	-.4936-02
.1546-01	-.3974-03	-.1327-01	-.2946-03
-.3235-07	.6967-05	.4427-03	-.4461-03

C Phasing Matrix, P_{C_5}

.1260-08	-.4643-03	.3315-00	.7077-01
.2728-02	.5299-08	-.1886+01	-.2069-00
.2015-01	.7210-04	-.0000	-.1373-01
-.0000	-.0000	-.0000	-.0000

By referring to the explicit dynamic equations given in the Appendix, the following observations can be made:

1. The instability appears very similar to classic pitch-lag instability [7] and is mainly a three-way coupling between first flatwise and edgewise bending modes and the rigid feathering degree-of-freedom. The resulting coupled mode, $\phi^{(3)}$ = (-0.383 - i0.435, 0.015 + i0.024, 1., -0.100 - i.0317).

2. The edgewise bending mode is being driven by inertia forces generated by flatwise bending motion: coriolis forces proportional to precone and flatwise bending rate and forces proportional to pitch angle and flatwise bending deflection.

3. The flatwise bending mode is being driven by aerodynamic forces generated chiefly by pitch-lag coupled edgewise bending and to a lesser extent rigid feathering deflection.

4. The rigid feathering degree-of-freedom is being driven principally by a centrifugal force moment involving chordwise mass radii of inertia, pitch angle, and edgewise bending rate.

The stiffness force-phasing matrices for this mode are formed and the significant terms for the edgewise bending equation are underlined:

A Phasing Matrix, $\hat{P}_{A_3}$

-.5097-00	.0000	.0000	.0000
.0000	-.3516-00	.0000	.0000
.0000	.0000	-.4455-00	.0000
.0000	.0000	.0000	-.1985-03

B Phasing Matrix, $\hat{P}_{B_3}$

.3425-02	.7927-03	.2799-01	.3780-02
-.3696-00	.1975-02	-.3394-00	-.1230-02
.1722-01	-.6235-03	.1190-03	-.9064-03
.1469-07	-.1870-05	-.1450-02	.3998-05

C Phasing Matrix, $\hat{P}_{C_3}$

.3382-00	.2803-02	.2923-00	-.1596-00
.1647-01	.1422+01	-.1179+01	.7995-00
-.1777-01	-.4505-04	.4431-00	.4327-02
.0000	.0000	.0000	.1646-02

It can be seen that the principal stiffening terms are, not unexpectedly, the diagonal mass and stiffness terms. The only other significant stiffening terms are those involving flatwise bending rate and deflection which are also the drivers of the unstable edgewise motion.

That the flatwise bending deflection term is negative and numerically greater than the rate dependent term can be appreciated by noting that the unstable coupled edgewise mode frequency, 1.324, is lower than the original corresponding stable mode frequency, 1.398.

V. Concluding Remarks

The "force-phasing" matrices technique provides yet another tool for understanding dynamic/aerodynamic phenomena. While it does not, by itself, indicate stability levels such as are provided by the eigensolution, it does complement the eigensolution by giving insight into the details of the dynamic configuration which are not directly available from the eigenvalues and eigenvectors alone. Moreover, the technique requires, in particular, eigenvector information as a starting point. Hence, it is inherently incapable of answering the more fundamental question of why, for any one mode, the eigenvector elements are indeed phased as they are. It should also be stressed that the technique is a tool to be used with, and in support of, engineer/analyst judgement; the results have to be interpreted properly, generally in the context of the specific application. Finally, the relative simplicity of the formulation makes the incorporation of the technique in any aeroelastic eigensolution program a straightforward and easily implemented task.

Appendix - Details of Dynamic Equations

The linear dynamic equations used to represent the aeroelastics of the rotor blade in hover are formulated using an assumed modal approach; the derivation is standard and uses the nomenclature of Reference 6. The linearization and subsequent simplifications are based upon the following assumptions:

1. quasi-static, incompressible, nonstalled airloads.
2. coincident spar center, shear center and tension center.
3. zero twist.
4. two flatwise bending modes, one edgewise bending mode and the rigid feathering degree-of-freedom.
5. normal uncoupled bending mode shapes (zero twist and pitch angle).

The flatwise bending equations are then written as:

$$\int_0^1 \Big\{ (\bar{m}\gamma_{w_i}\gamma_{w_m})\,\ddot{q}_{w_m} + (\bar{m}\,\bar{y}_{1O_{cg}}\gamma_{w_i}\gamma_{\theta_j})\,\ddot{q}_{\theta_j} + [2\bar{m}\gamma_{w_i}(\beta\gamma_{v_k} + \bar{y}_{1O_{cg}}\sin\theta\gamma'_{v_k})]\,\dot{q}_{v_k} - (2\,\bar{m}\,\bar{k}^2_{y_{1O}}\cos\theta\,\gamma_{\theta_j}\gamma'_{w_i})\,\dot{q}_{\theta_j} + [\overline{EI}_y\gamma''_{w_i}\gamma''_{w_m} + \bar{T}\gamma'_{w_i}\gamma'_{w_m} - \bar{m}\sin^2\theta\,\gamma_{w_i}\gamma_{w_m}]\,q_{w_m} + (\bar{m}\gamma_{w_i}\gamma_{v_k}\sin\theta\cos\theta)\,q_{v_k} + [\bar{m}\gamma_{w_i}(\bar{y}_{1O_{cg}}\cos 2\theta - \bar{r}\beta\sin\theta)\gamma_{\theta_j}]\,q_{\theta_j} + \frac{\rho acR}{2m_o}\gamma_{w_i}\big[-\bar{r}^2\big(\gamma_{\theta_j}q_{\theta_j} + A_{w_m}q_{w_m} + A_{v_k}q_{v_k}\big) + \bar{r}\big(\gamma_{w_m}\dot{q}_{w_m} + \bar{y}_{1O_{3c/4}}(\gamma_{\theta_j}\dot{q}_{\theta_j} + A_{w_m}\dot{q}_{w_m} + A_{v_k}\dot{q}_{v_k}) - \alpha_o\gamma_{v_k}\dot{q}_{v_k}\big)\big]\Big\}\,d\bar{r} = 0 \qquad \text{(A-1)}$$

The edgewise equations are written as:

$$\int_0^1 \Big\{ (\bar{m}\gamma_{v_k}\gamma_{v_n})\ddot{q}_{v_n}$$

$$-[2\,\bar{m}\gamma_{w_m}(\beta\gamma_{v_k} + \bar{y}_{10_{cg}}\sin\theta\,\gamma'_{v_k})]\,\dot{q}_{w_m}$$

$$-[2\,\bar{m}(\beta\bar{y}_{10_{cg}}\gamma_{v_k} + \bar{k}^2_{z_{10}}\sin\theta\,\gamma'_{v_k})\,\gamma_{\theta_j}]\,\dot{q}_{\theta_j}$$

$$+(\bar{m}\gamma_{v_k}\gamma_{w_m}\sin\theta\,\cos\theta)\,q_{w_m} \qquad \text{(A-2)}$$

$$+[\overline{EI}_z\gamma''_{v_k}\gamma''_{v_n} + \bar{T}\gamma'_{v_k}\gamma'_{v_n} - \bar{m}\cos^2\theta\,\gamma_{v_k}\gamma_{v_n}]\,q_{v_n}$$

$$+[\bar{m}\gamma_{v_k}(\bar{r}\beta\,\cos\theta + \bar{y}_{10_{cg}}\sin 2\theta)\gamma_{\theta_j}]\,q_{\theta_j}$$

$$+\frac{\rho acR}{2m_o}\gamma_{v_k}\Big[-\bar{r}^2(2\,\alpha_o - 4\,\frac{\delta_4}{a}\alpha_o^3)(\gamma_{\theta_j}q_{\theta_j} + A_{w_m}q_{w_m}$$

$$+ A_{v_n}q_{v_n}) + \bar{r}(2\,\alpha_o - 4\,\frac{\delta_4}{a}\alpha_o^3 - 2\,\frac{\delta_o}{a}\theta)\Big(\gamma_{w_m}\dot{q}_{w_m}$$

$$+ \bar{y}_{10_{3c/4}}(\gamma_{\theta_j}\dot{q}_{\theta_j} + A_{w_m}\dot{q}_{w_m} + A_{v_n}\dot{q}_{v_n})\Big)$$

$$+ 2\,\bar{r}(\frac{\delta_o}{a} - \frac{\delta_4}{a}\alpha_o^4)\gamma_{v_n}\dot{q}_{v_n}\Big]\Big\}d\bar{r} + C_{e_k}\dot{q}_{v_k} = 0$$

The torsion equations are written as:

$$\int_0^1 \Big\{ (\bar{m}\,\bar{y}_{10_{cg}}\gamma_{\theta_j}\gamma_{w_m})\ddot{q}_{w_m} + [\bar{m}(\bar{k}^2_{y_{10}} + \bar{k}^2_{z_{10}})\gamma_{\theta_j}\gamma_{\theta_k}]\ddot{q}_{\theta_k}$$

$$+(2\,\bar{m}\,\bar{k}^2_{y_{10}}\cos\theta\,\gamma_{\theta_j}\gamma'_{w_m})\,\dot{q}_{w_m}$$

$$+[2\,\bar{m}(\beta\bar{y}_{10_{cg}}\gamma_{v_n} + \bar{k}^2_{z_{10}}\sin\theta\,\gamma'_{v_n})\,\gamma_{\theta_j}]\,\dot{q}_{v_n}$$

$$+[\bar{m}\,\bar{y}_{10_{cg}}(\bar{r}\gamma'_{w_m} - \sin^2\theta\,\gamma_{w_m})\gamma_{\theta_j}]\,q_{w_m}$$

$$+[(\overline{GJ} + \bar{k}^2\bar{A}\bar{T})\,\gamma'_{\theta_j}\gamma'_{\theta_k} + \bar{m}(\bar{k}^2_{z_{10}} - \bar{k}^2_{y_{10}})\cos 2\theta\,\gamma_{\theta_j}\gamma_{\theta_k}]q_{\theta_k}$$

$$+(\bar{m}\,\bar{y}_{10_{cg}}\sin\theta\,\cos\theta\,\gamma_{\theta_j}\gamma_{v_n})\,q_{v_n} \qquad \text{(A-3)}$$

$$+\frac{\rho acR}{2m_o}\gamma_{\theta_j}[-\bar{r}^2\bar{y}_{10_{c/4}}(\gamma_{\theta_k}q_{\theta_k} + A_{w_m}q_{w_m} + A_{v_n}q_{v_n})$$

$$+\bar{r}\,\bar{y}_{10_{c/4}}\Big(\gamma_{w_m}\dot{q}_{w_m} - \alpha_o\gamma_{v_n}\dot{q}_{v_n} + \bar{y}_{10_{3c/4}}(\gamma_{\theta_k}\dot{q}_{\theta_k}$$

$$+ A_{w_m}\dot{q}_{w_m} + A_{v_n}\dot{q}_{v_n})\Big) - \frac{\pi c}{2aR}\bar{r}\,\bar{y}_{10_{3c/4}}(\gamma_{\theta_k}\dot{q}_{\theta_k}$$

$$+ A_{w_m}\dot{q}_{w_m} + A_{v_n}\dot{q}_{v_n})]\Big\}d\bar{r} + \frac{K_c\delta_{j,1}}{m_o R^3\Omega^2}q_{\theta_1} = 0$$

where:

$$\alpha_o = \theta + \lambda/\bar{r} \qquad \text{(A-4)}$$

References

1. Wilkinson, J. H.: The Algebraic Eigenvalue Problem. Clarendon Press, Oxford, 1965.

2. Programmer's Manual: Subroutines ATEIG and HSBG. IBM System/360 Scientific Subroutine Package, Version III, GH20-0205-4, August 1970.

3. Leppert, E. L., Jr.: A Fraction Series Solution for Characteristic Values Useful in Some Problems of Airplane Dynamics. Journal of the Aeronautical Sciences, Vol. 22, No. 5, May 1955.

4. Bielawa, R. L.: Techniques for Stability Analysis and Design Optimization with Dynamic Constraints of Nonconservative Linear Systems. AIAA/ASME 12th Structures, Sturctural Dynamics and Materials Conference Paper No. 71-388, Anaheim, California, April 1971.

5. Miller, R. H. and C. W. Ellis: Blade Vibration and Flutter. Journal of the American Helicopter Society, Vol. 1, No. 3, July 1956.

6. Arcidiacono, P. J.: Prediction of Rotor Instability at High Forward Speeds. Vol. I, Differential Equations of Motion for a Flexible Helicopter Rotor Blade in Steady Flight Including Chordwise Mass Unbalance Effects. USAAVIABS Technical Report 68-18A, U. S. Army, February 1969.

7. Chou, P. C.: Pitch-Lag Instability of Helicopter Rotors. Journal of the American Helicopter Society, Vol. 3, No. 3, July 1958.